Texture and Anisotropy of Hot-Pressed h-BN Matrix Composite Ceramics With in Situ Formed YAG

Zhuo Zhang
Harbin Institute of Technology
Xiaoming Duan (duanxiaoming@hit.edu.cn)
Harbin Institute of Technology https://orcid.org/0000-0002-8723-8286
Zhuo Tian
Guangdong University of Technology
Yujin Wang
Harbin Institute of Technology
Lan Wang
Harbin Institute of Technology
Lei Chen
Harbin Institute of Technology
Baofu Qiu
Harbin Institute of Technology
Delong Cai
Harbin Institute of Technology
Peigang He
Harbin Institute of Technology
Dechang Jia
Harbin Institute of Technology
Yu Zhou
Harbin Institute of Technology

Research Article

Keywords: Hexagonal boron nitride, Liquid phase sintering, Texture, Anisotropy

Posted Date: August 26th, 2021

DOI: https://doi.org/10.21203/rs.3.rs-839901/v1

Version of Record: A version of this preprint was published at Journal of Advanced Ceramics on March 17th, 2022. See the published version at https://doi.org/10.1007/s40145-021-0553-3.

Texture and anisotropy of hot-pressed h-BN matrix composite ceramics with *in situ* formed YAG

Zhuo Zhang[a,b], Xiaoming Duan[a,b,c,*], Zhuo Tian[d], Yujin Wang[a,b,*], Lan Wang [a,b], Lei Chen[a,b], Baofu Qiu[a,b], Delong Cai[a,b], Peigang He[a,b], Dechang Jia[a,b,c,*], Yu Zhou[a,b]

[a]Key Laboratory of Advanced Structural-Functional Integration Materials & Green Manufacturing Technology, Harbin Institute of Technology, Harbin, 150001, China

[b]Institute for Advanced Ceramics, School of Materials Science and Engineering, Harbin Institute of Technology, Harbin, 150001, China

[c]State Key Laboratory of Advanced Welding and Joining, Harbin Institute of Technology, Harbin, 150001, China

[d]School of Electromechanical Engineering, Guangdong University of Technology, Guangzhou 510006, Guangdong, China

Abstract

Textured h-BN matrix composite ceramics were prepared by hot-pressing using different contents of $3Y_2O_3$-$5Al_2O_3$ (mole ratio of 3:5) as the liquid phase sintering additive. During the hot-pressing process, the liquid $Y_3Al_5O_{12}$ (YAG) phase with good wettability to h-BN grains was *in situ* formed through the reaction between Y_2O_3 and Al_2O_3, and a coherent relationship between h-BN and YAG was observed with $[010]_{h\text{-}BN}$ // $[\bar{1}11]_{YAG}$ and $(002)_{h\text{-}BN}$ // $(321)_{YAG}$. Plate-like h-BN grains in the YAG liquid phase environment were rotated under the action of the uniaxial sintering pressure, making their basal surfaces preferentially arranged perpendicular to the sintering pressure, forming textured microstructures with the *c*-axis of h-BN grains oriented parallel to the sintering pressure, which give these composite ceramics anisotropy in their mechanical and thermal properties. The highest texture degree was

* Corresponding author: Tel.: +86 451 86418792; fax: +86 451 86414291. E-mail *addresses*: duanxiaoming@hit.edu.cn, dxmhit@126.com (Xiaoming Duan); wangyuj@hit.edu.cn (Yujin Wang); dcjia@hit.edu.cn (Dechang Jia).

found in the specimen with 30 wt.% YAG content, which also possesses the most anisotropic thermal conductivity. The aggregation of YAG phase resulting in the buckling of h-BN plates was observed in the specimen with 40 wt.% YAG content, which significantly reduced its texture degree.

Key words:

Hexagonal boron nitride; Liquid phase sintering; Texture; Anisotropy.

1. Introduction

Hexagonal boron nitride (h-BN) has a layered structure similar to that of graphite, where B and N atoms are combined by covalent bonds with *sp2* hybridization in the same layer, while different layers are combined by van der Waals forces [1-3]. Due to its unique crystal structure, the single h-BN crystal shows anisotropy in the physical properties. Its elastic moduli along the *a, b*-axis and the *c*-axis were calculated to be 837.99 GPa and 33.40 GPa, respectively [4, 5], giving textured h-BN ceramics anisotropic mechanical properties [6]. Its theoretical thermal conductivity parallel and perpendicular to the *c*-axis was calculated to be 4.1 W/(m·K) and 537 W/(m·K), respectively [7], coupled with its insulating property [8], making h-BN matrix composites promising thermal management devices in electronics [9-14].

The strong *sp2* covalent bonds combining B and N atoms result in a very low atomic diffusion rate even at high sintering temperatures, which makes h-BN ceramics hard to be densified during sintering [15, 16]. Introducing sintering additives composed of two or more oxides, such as Y_2O_3-Al_2O_3, Y_2O_3-SiO_2, Yb_2O_3-MgO,

Yb-Si-Al(N)-O, La-Al-Si-O, etc. [17-23], has been widely proven to be an effective method to improve the sinterability of h-BN ceramics as these oxides can form liquid phases at high sintering temperatures and fill these pores between plate-like h-BN grains with the "house of cards" structure.

Compared with plate-like h-BN powders having large grain sizes, fine h-BN powders with more defects are more easily to be densified due to their high surface energy and defect energy [24, 25]. However, the final gain size of h-BN ceramics prepared using fine h-BN powders is limited even with liquid phase sintering additives [26-28], thus h-BN ceramics with a significant texture cannot be obtained. Plate-like h-BN powders with larger grain sizes and liquid phase sintering additives are still necessary for the fabrication of textured h-BN matrix composite ceramics with significant anisotropy.

In our previous work, the textured h-BN matrix composite specimen with an index of orientation preference (*IOP*) of -530 was prepared by hot-pressing using 20 wt.% $3Y_2O_3$-$5Al_2O_3$ with a mole ratio of 3:5 as the sintering additive, which can transform into YAG phase showing good wettability to h-BN grains [19]. In this paper, Different contents (10 wt.%, 20 wt.%, 30 wt.% and 40 wt.%) of $3Y_2O_3$-$5Al_2O_3$ were used to prepare h-BN matrix composite ceramics by hot-pressing to investigate the influence of YAG contents on the texture and anisotropy in the mechanical and thermal properties of the composite ceramics.

2. Materials and methods

The raw materials were h-BN powders with a platelike morphology (~15 μm in

diameter and ~0.3 μm in thickness, purity > 99%), α-Al_2O_3 powders (~0.2 μm, purity > 99.9%) and Y_2O_3 powders (~2 μm, purity > 99.9%). $3Y_2O_3$-$5Al_2O_3$ (mole ratio of 3:5) were used as the sintering additive. The mass ratios of h-BN to the sintering additive were 9:1, 8:2, 7:3 and 6:4, respectively. Raw powders were mixed using Al_2O_3 balls in ethanol on a pot-mill machine with a rotation speed of 80 rpm for 24 h and then dried on a hot plate set at 70 °C. Mixed powders were loaded into a *Φ*50 mm cylindrical graphite die and hot-pressed at 1900 °C under a uniaxial pressure of 30 MPa in N_2 atmosphere for 1 h. The hot-pressed h-BN matrix composite ceramics with 10 wt.%, 20 wt.%, 30 wt.% and 40 wt.% YAG contents (it will be proven in part 3.1 that Y_2O_3 and Al_2O_3 fully reacted during hot-pressing, forming YAG with a cubic crystal structure) were marked as BN-1YAG, BN-2YAG, BN-3YAG and BN-4YAG, respectively.

Bulk densities of the hot-pressed specimens were measured by Archimedes method. The phase compositions and crystallographic orientation of the specimens were analyzed by X-ray diffraction (XRD; X′PERT, Panalytical, Netherlands). Further analysis on phases and interface microstructure were realized by transmission electron microscopy (TEM; Tecnai G2 F30, FEI, USA). Mechanical properties were measured along three different loading directions by the electronic universal testing machine (Model 5569, Instron, USA): flexural strength was tested on 3 mm × 4 mm × 36 mm sample bars by three-point bending with a span of 30 mm and a crosshead speed of 0.5 mm/min; elastic moduli were tested using strain gauges stuck on the tensile surfaces of the strength sample bars; fracture toughness was tested on 2 mm ×

4 mm × 20 mm single-edge-notched beams with a span of 16 mm and a crosshead speed of 0.05 mm/min. Fracture morphologies were observed using scanning electron microscopy (SEM; Quanta 200 FEG, FEI, USA). Thermal expansion coefficients were measured on 5 mm × 5 mm × 25 mm bars using thermal expansion instrument (DTL 402C, Netzsch, Germany). Specific heat capacity and thermal diffusivity were measured on Φ 12.7 mm × 2~3 mm discs by laser flash method (LFA 427, Netzsch, Germany) and thermal conductivity was calculated from them.

3. Results and discussion

3.1. Phase compositions, texture and interface microstructure

Fig. 1 shows the XRD patterns measured on both top surfaces (TS) perpendicular to the sintering pressure and side surfaces (SS) parallel to the sintering pressure of these h-BN matrix composite ceramics hot-pressed using different contents of the $3Y_2O_3$-$5Al_2O_3$ additive. All the four specimens are composed of two phases: h-BN and YAG, indicating that Y_2O_3 and Al_2O_3 have reacted sufficiently with the molar ratio of 3:5. They all show a significantly higher h-BN(002) diffraction peak for TS than that for SS and a higher h-BN(100) diffraction peak for SS than that for TS, indicating that all specimens possess textured microstructures with the *c*-axis of h-BN grains preferentially arranged parallel to the sintering pressure, which were attributed to the rotation of plate-like h-BN grains under the action of the uniaxial sintering pressure in the YAG liquid phase environment.

Fig. 2 gives the relative densities, indexes of orientation preference (*IOP*) and Lotgering orientation factors f_{00l} of the hot-pressed h-BN matrix composite ceramics

with different YAG contents. The relative density increases with the increase of the YAG content and reach the highest for BN-4YAG (92.36%), as the liquid YAG phase acted as a gap filler in the "house of cards" structure formed by plate-like h-BN grains during hot-pressing.

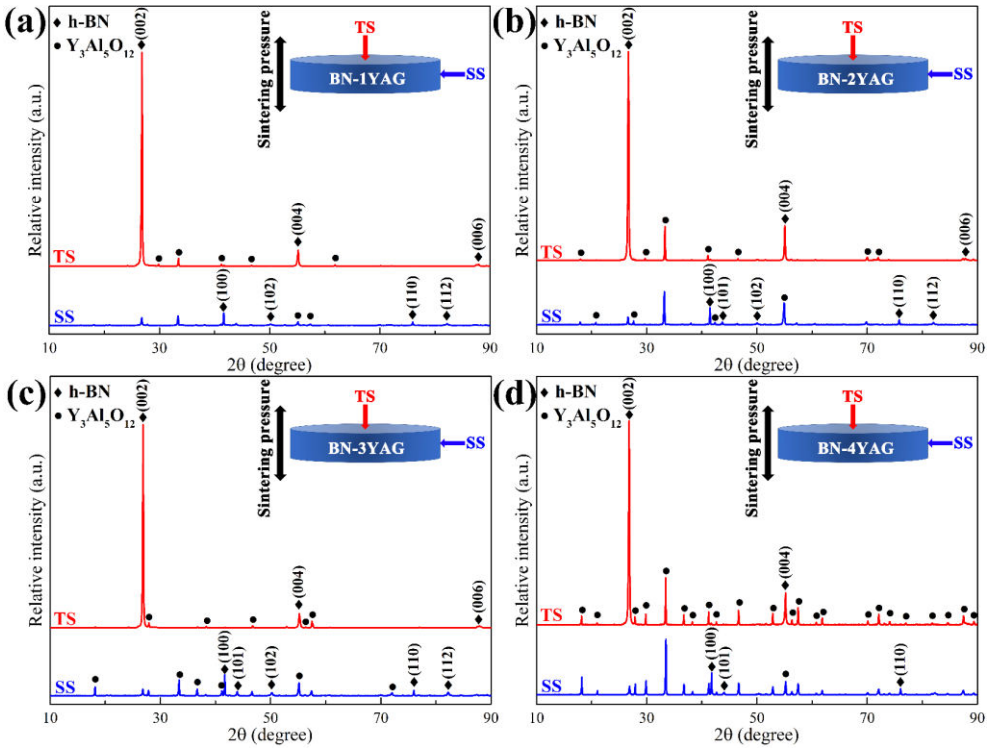

Fig. 1. XRD patterns for TS and SS of the hot-pressed h-BN matrix composite ceramics with different YAG contents: (a) 10 wt.%; (b) 20 wt.%; (c) 30 wt.%; (d) 40 wt.%.

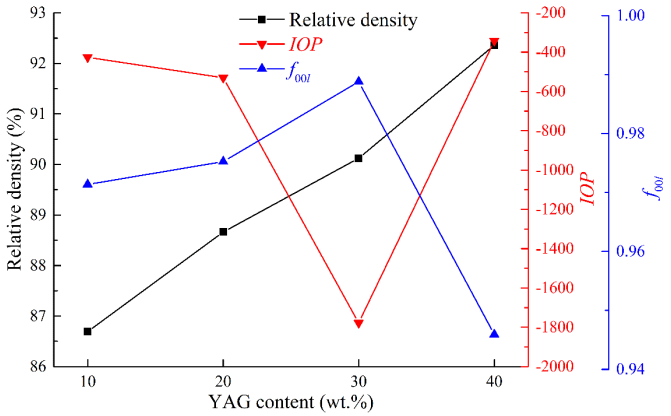

Fig. 2. Relative densities, *IOP* and f_{00l} of the hot-pressed h-BN matrix composite ceramics with different YAG contents.

IOP and f_{00} are used to quantitively characterize the texture degree of h-BN matrix composite ceramics. *IOP* can be calculated by Eq. (1) [29]:

$$IOP = \begin{cases} \dfrac{(I_{100}/I_{002})\mathrm{TS}}{(I'_{100}/I'_{002})\mathrm{SS}}, \text{When } (I_{100}/I_{002})\mathrm{TS} > (I'_{100}/I'_{002})\mathrm{SS} \\ -\dfrac{(I'_{100}/I'_{002})\mathrm{SS}}{(I_{100}/I_{002})\mathrm{TS}}, \text{When } (I_{100}/I_{002})\mathrm{TS} < (I'_{100}/I'_{002})\mathrm{SS} \end{cases} \quad (1)$$

where I_{hkl} and I'_{hkl} are the intensities of (*hkl*) diffraction peaks for TS and SS, respectively. For a hot-pressed h-BN matrix composite specimen, *IOP* = ±1 indicates that it consists of randomly oriented h-BN grains; *IOP* < -1 and *IOP* > 1 indicate that its h-BN grains are preferentially oriented with the *c*-axis parallel and perpendicular to the uniaxial sintering pressure, respectively. In this paper, a negative *IOP* with a larger absolute value indicates a higher texture degree.

f_{00l} can be calculated according to Eqs. (2, 3) [30]:

$$f_{00l} = \frac{P - P_0}{1 - P_0} \quad (2)$$

$$P \text{ and } P_0 = \frac{\sum I_{00l}}{\sum I_{hkl}} \quad (3)$$

where $\sum I_{00l}$ and $\sum I_{hkl}$ are the sums of the diffraction peak intensities of all (00*l*) and (*hkl*) planes, respectively; *P* was calculated from the measured XRD patterns for TS, on which (00*l*) planes are preferentially oriented, of the hot-pressed specimens, while P_0 was calculated from the standard JCPDS card (PDF#34-0421) of h-BN. *P* is always lower than 1, thus f_{00l} is always lower than 1. A higher f_{00l} closer to 1 indicates more (00*l*) planes on TS.

With the increase of the YAG content in the hot-pressed h-BN matrix composite ceramics, the absolute values of *IOP* and f_{00l} both increase first and then decrease dramatically, and reach the highest for BN-3YAG (*IOP* = -1778; f_{00l} = 0.99), which

means that BN-3YAG has the highest texture degree.

Fig. 3 displays the bright field images and selected area electron diffraction (SAED) patterns for SS of BN-3YAG and BN-4YAG. These plate-like h-BN grains are well oriented with their (002) planes perpendicular to SS for BN-3YAG, which is confirmed by the diffraction pattern of area A in Fig. 3(a). The diffraction pattern of area B shows a secondary diffraction pattern caused by h-BN below the YAG area, and there are a row of diffraction spots deviating from the marked (002) spots, which could be caused by the orientation deviation of adjacent h-BN grains. The arrangement of h-BN grains in BN-4YAG is not as orderly as that in BN-3YAG, which is demonstrated by the existence of both $(1\bar{1}0)$ planes (area A in Fig. 3(b)) and (002) planes (area B in Fig. 3(b)) of h-BN grains. The aggregation of liquid YAG phase (area C in Fig. 3(b)) caused the buckling of plate-like h-BN grains, which significantly reduced the texture degree of BN-4YAG.

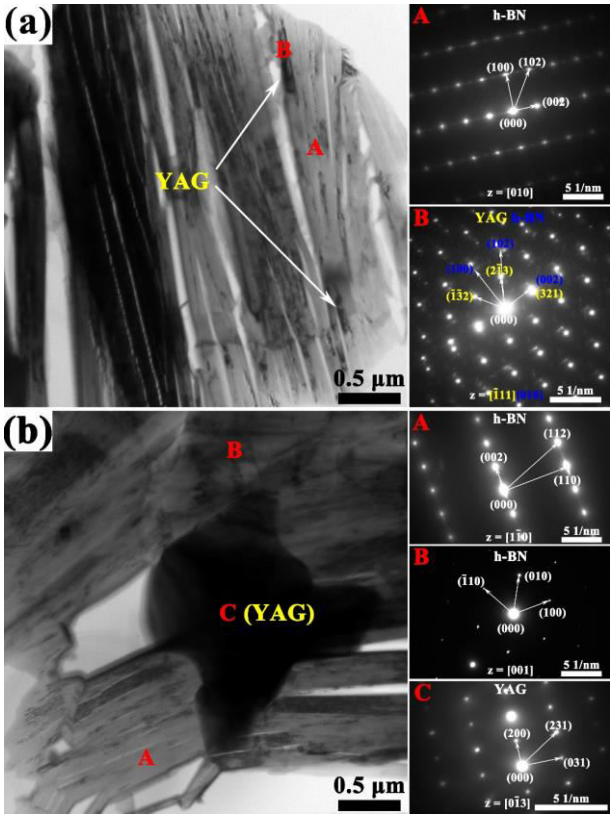

Fig. 3. The bright field images and SAED patterns for SS of (a) BN-3YAG and (b) BN-4YAG, respectively.

Fig. 4 shows the HRTEM image, FFT pattens and IFFT images around the interface between h-BN and YAG in BN-3YAG. Areas 1~4 are h-BN, the interface between h-BN and YAG, YAG and the h-BN area infiltrated by YAG, respectively. Stacking fault was observed in h-BN (Fig. 4(b)), which has been proved to commonly exist due to the "multi-area co-growth" of h-BN grains in our previous work [26].

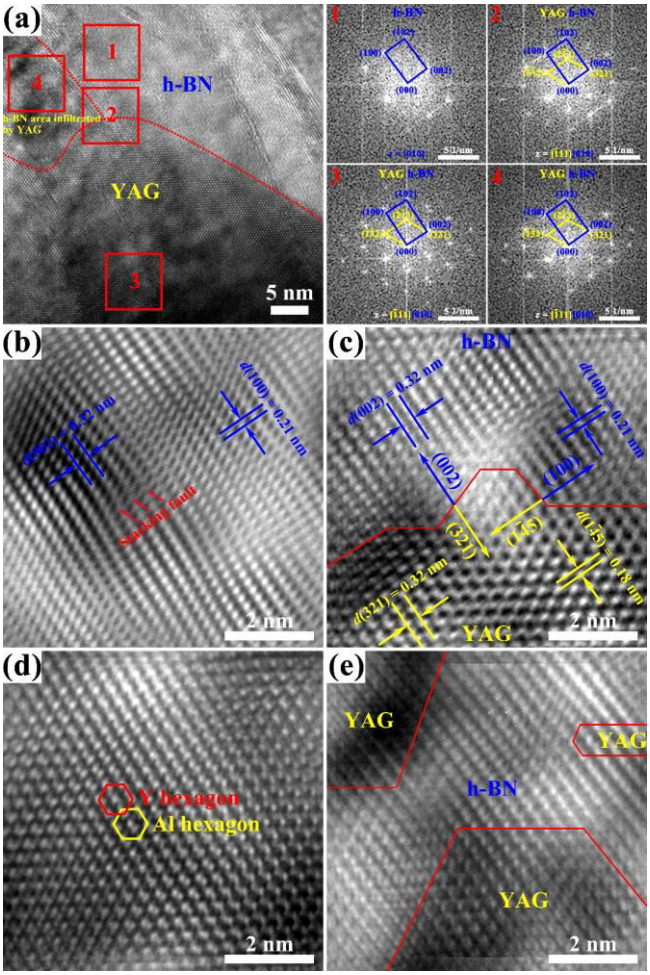

Fig. 4. The HRTEM image, FFT pattens and IFFT images around the interface between h-BN and YAG in BN-3YAG: (a) HRTEM images and FFT patterns corresponding to areas 1~4; (b~e) IFFT images corresponding to areas 1~4 in (a).

The IFFT image of area 2 displays the coherent interface between h-BN and YAG (Fig. 4(c)), where the (002) and (100) planes of h-BN are parallel to the (321) and $(1\bar{4}5)$ planes of YAG, respectively. The IFFT image of area 3 displays the crystal structure of YAG observed from the $[\bar{1}11]$ direction (Fig. 4(d)), where the hexagons composed of Al and Y atoms are easily distinguished, while the secondary diffraction pattern in the FFT pattern of area 3 confirms the existence of h-BN below the well-crystallized YAG. The FFT pattern and IFFT image of area 4, where the YAG phase infiltrates into the h-BN grain from multiple directions, further

demonstrate the good wettability of YAG to h-BN grains (Fig. 4(e)).

Fig. 5(a) shows the schematic diagrams of the fracture modes and the fracture morphologies along different loading directions (D1, D2 and D3) of the hot-pressed h-BN matrix composite ceramics with different YAG contents. For D1, the long axis of the sample bar is perpendicular to the h-BN layers (parallel to the *c*-axis orientation) and the loading direction is parallel to the h-BN layers, resulting in a relative flat fracture surface. For D2, the long axis of the sample bar is parallel to the h-BN layers and the loading direction is perpendicular to the h-BN layers, resulting in a tortuous crack propagation path. For D3, the long axis of the sample bar is parallel to the h-BN layers and the loading direction is also parallel to the h-BN layers, generating a tortuous initial crack and a fracture morphology similar to that along D2.

The fracture morphologies of BN-3YAG show the most significant texture (Fig. 5(h~j)), which is in consistent with the XRD results. For BN-1YAG, the side of the (002) plane of h-BN was observed on the fracture morphology along D1, and the (002) plane of h-BN was observed on the fracture morphology along D2 and D3. For BN-4YAG, many buckling behaviors of h-BN plates were observed (Fig. 5(k~m)), which have been proved to be caused by the aggregation of liquid YAG phase (Fig. 3(b)) and significantly reduced its texture degree.

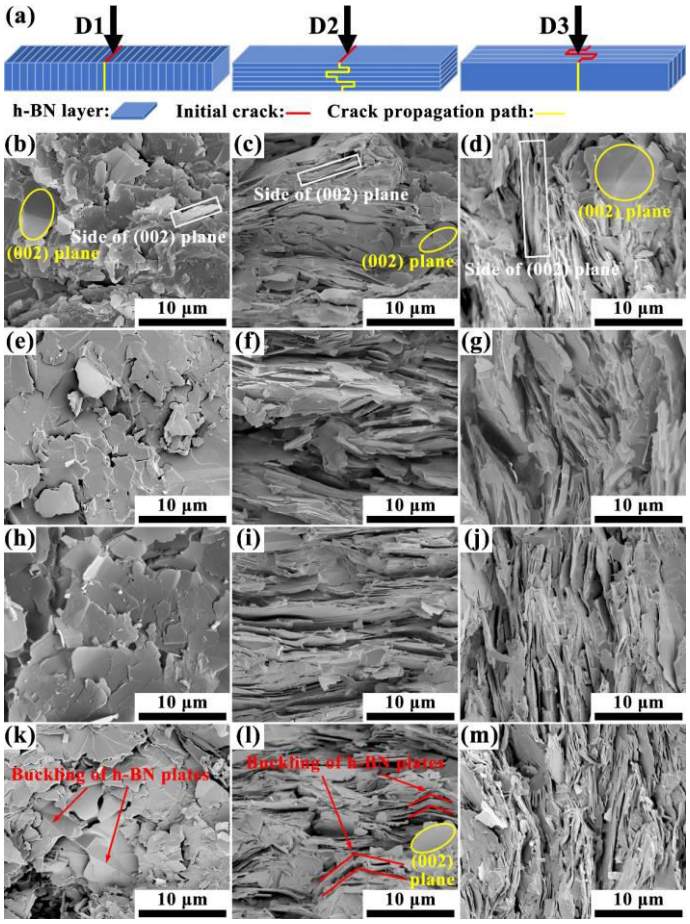

Fig. 5. Schematic diagrams of the fracture modes and fracture morphologies of the hot-pressed h-BN matrix composite ceramics with different YAG contents: (a) Schematic diagrams of the fracture modes along D1, D2 and D3; (b~d), (e~g), (h~j) and (k~m) Fracture morphologies along D1, D2, D3 of BN-1YAG, BN-2YAG, BN-3YAG and BN-4YAG, respectively.

3.2. Anisotropic properties

Fig. 6 gives the mechanical properties of the hot-pressed h-BN matrix composite ceramics with different YAG contents. The work of fracture (γ_{WOF}) was calculated from the load-displacement curves during the fracture toughness testing according to Eq. (4) [31]:

$$\gamma_{WOF} = \frac{\int F d\delta}{2A} \tag{4}$$

where $\int F d\delta$ is the total fracture energy during the fracture toughness testing and was determined as the area under the load-displacement curves; A is the

cross-sectional area of the unnotched part of the single-edge-notched beams.

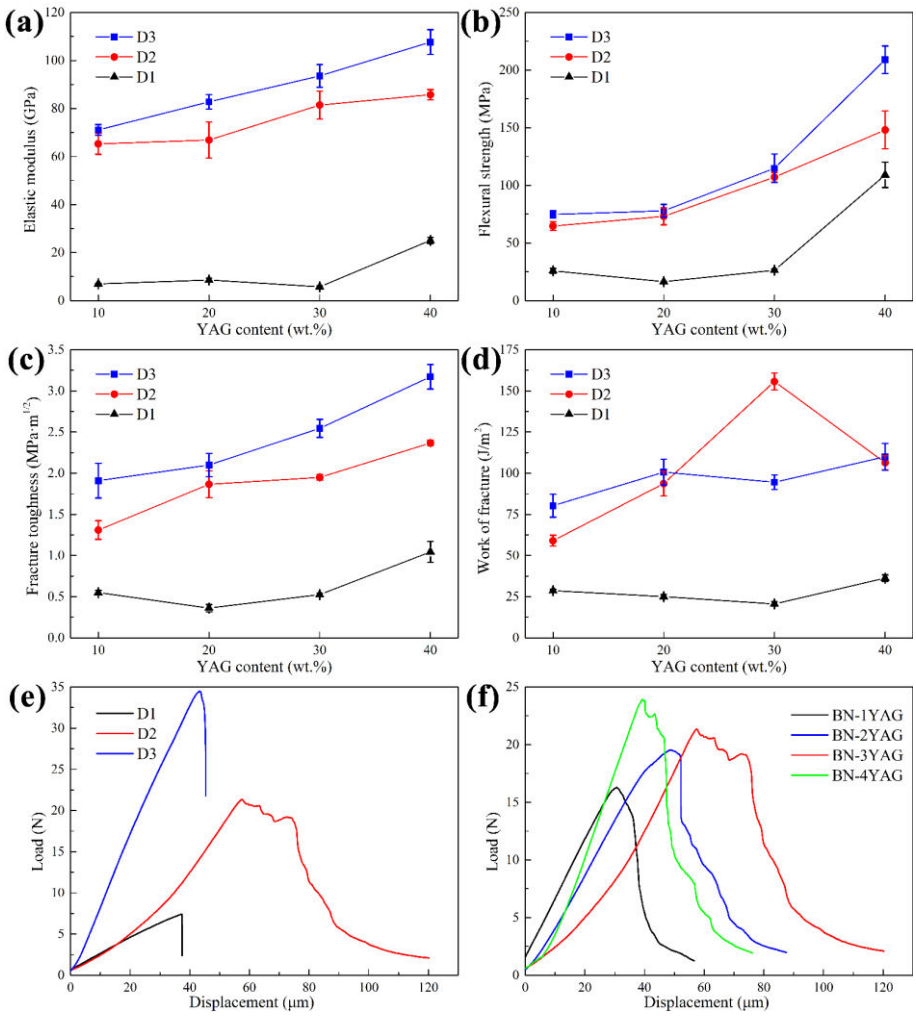

Fig. 6. Mechanical properties of the hot-pressed h-BN matrix composite ceramics with different YAG contents: (a) Elastic moduli; (b) Flexural strength; (c) Fracture toughness; (d) Work of fracture; (e) Load-displacement curves along D1, D2 and D3 of BN-3YAG; (f) Load-displacement curves along D2 of the specimens with different YAG contents.

As the *sp2* covalent bonds combining B and N atoms in the same layer are much stronger than the van der Waals forces between different layers, the mechanical properties along D1 of these hot-pressed h-BN matrix composite ceramics are much lower than that along D2 and D3. The elastic moduli, flexural strength and fracture toughness along D3 of these specimens with different YAG contents are all a little

higher than that along D2, which could be attributed to that the crack initiation along D2 only needs to break the *sp2* covalent bonds combining B and N atoms, while the crack initiation along D3 needs to break both the *sp2* covalent bonds combining B and N atoms and the van der Waals forces between different layers.

The elastic moduli increase with the increase of the YAG content along D2 and D3 even for BN-4YAG whose texture degree was dramatically reduced, which is attributed to the high isotropic elastic moduli (~300 GPa) of polycrystalline YAG ceramics with a cubic crystal structure [32]. While the elastic modulus along D1 of BN-3YAG is lower than that of BN-2YAG due to its higher texture degree. Flexural strength and fracture toughness show similar trends. Therefore, both the orientation of h-BN grains (texture degree) and the properties of YAG phase contribute to the mechanical properties of the hot-pressed h-BN matrix composite ceramics.

For h-BN matrix composite ceramics with relatively lower texture degrees (BN-1YAG, BN-2YAG and BN-4YAG), the work of fracture along D2 is lower than that along D3, which is in consistent with the fracture toughness. However, for BN-3YAG, its work of fracture along D2 (155.7 ± 5.1 J/m^2) is much higher than that along D3 (94.5 ± 4.5 J/m^2) despite its lower fracture toughness along D2 than that along D3, which owes to its high texture degree and more tortuous crack propagation path along D2. Fig. 6(e) shows the load-displacement curves along D1, D2 and D3 of BN-3YAG during the fracture toughness testing. The highest load along D3 is higher than that along D2, leading to the higher fracture toughness along D3 than that along D2. BN-3YAG behaved a non-catastrophic fracture mode along D2 due to the

orientation of plate-like h-BN grains, which resulted in the step-by-step decrease of load with the increase of displacement during the tortuous crack propagation. Such a non-catastrophic fracture mode was also observed in the load-displacement curves along D2 of other specimens (Fig. 6(f)). Fig. 7 shows the lateral fracture morphologies along D2 of the hot-pressed h-BN matrix composite ceramics with different YAG contents, where crack deflection phenomena correspond to the step-by-step decrease of load with the increase of displacement during crack propagation. Different from BN-3YAG, the texture degrees of other specimens are not that high to induce crack propagation paths tortuous enough which can give them higher work of fracture along D2 than that along D3.

Fig. 8 shows the linear thermal expansion curves and coefficients of thermal expansion (CTE) measured parallel and perpendicular to the *c*-axis orientation of the hot-pressed h-BN matrix composite ceramics with different YAG contents. It has been calculated that the CTE of YAG at room temperature is around 7×10^{-6}/K [33], and that perpendicular to the *c*-axis of h-BN is -2.72×10^{-6}/K at room temperature and approaches zero at high temperatures, while that parallel to the *c*-axis of h-BN is 37.7×10^{-6}/K at room temperature and tends to be invariable at high temperatures [34]. The contribution of YAG makes the anisotropy degrees in the thermal expansion of the composite ceramics not totally consistent with their texture degrees. Although BN-2YAG has a higher texture degree than BN-1YAG, the anisotropy degree of CTE of BN-2YAG is lower than that of BN-1YAG, which is caused by the higher CTE of YAG than that perpendicular to the *c*-axis of h-BN.

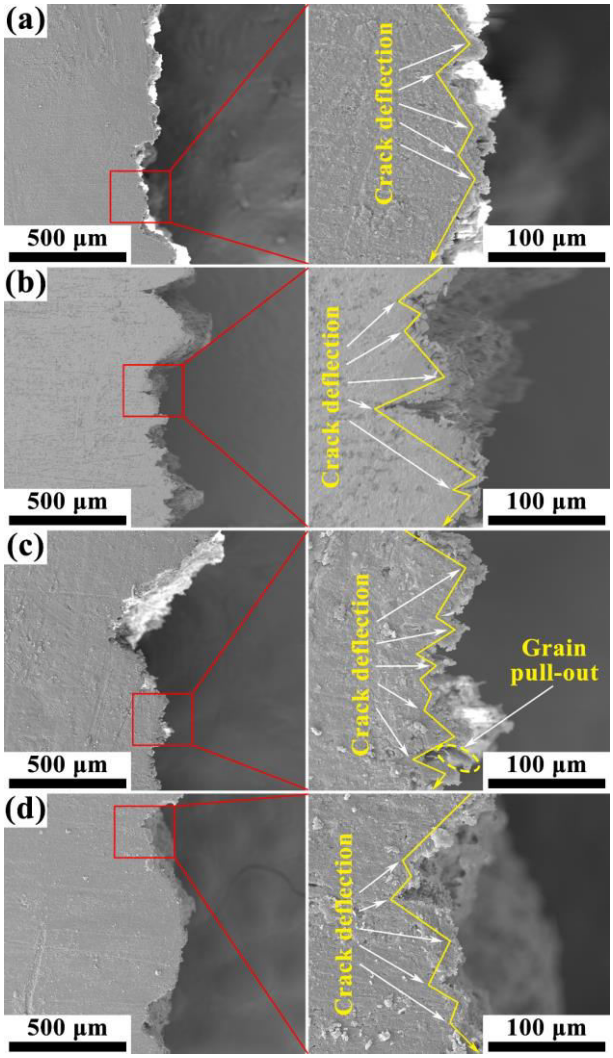

Fig. 7. Lateral fracture morphologies along D2 of (a) BN-1YAG, (b) BN-2YAG, (c) BN-3YAG and (d) BN-4YAG, respectively.

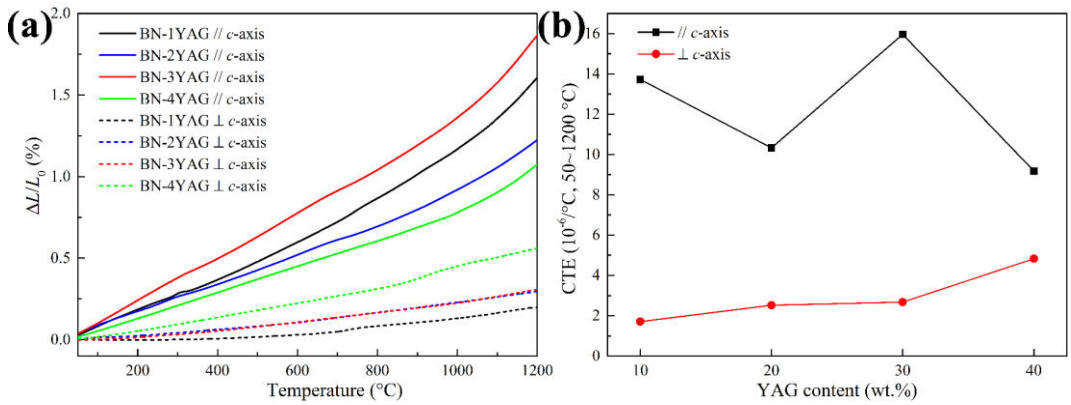

Fig. 8. (a) Linear thermal expansion curves and (b) CTE measured parallel and perpendicular to the *c*-axis orientation of the hot-pressed h-BN matrix composite ceramics with different YAG contents.

Fig. 9 gives the thermal diffusivity and thermal conductivity (25~1200 °C)

parallel and perpendicular to the *c*-axis orientation of the hot-pressed h-BN matrix composite ceramics with different YAG contents and their anisotropy degrees in thermal conductivity, which were determined by the ratio of the thermal conductivity perpendicular to the *c*-axis orientation to that parallel to the *c*-axis orientation.

All specimens have higher thermal conductivity perpendicular to the *c*-axis orientation than that parallel to the *c*-axis orientation due to the anisotropic thermal conductivity of h-BN [7]. BN-3YAG has the highest thermal diffusivity (82.4 mm^2/s at 25 °C) and thermal conductivity (163.2 W/(m·K) at 25 °C) perpendicular to the *c*-axis orientation due to its highest texture degree, which are 11.1 times of that (7.4 mm^2/s and 14.7 W/(m·K)) parallel to the *c*-axis orientation at room temperature. Although having the highest texture degree, BN-3YAG has higher thermal conductivity parallel to the *c*-axis orientation than BN-2YAG (11.7 W/(m·K) at 25 °C), which is attributed to its higher relative density.

The thermal diffusivity and thermal conductivity decrease and the decrease rate gets slower with increasing the testing temperature (Fig. 9(a, b)), especially for the direction parallel to the *c*-axis orientation of these composite ceramics, which is caused by the influence of temperature on the mean free path of phonons. As the thermal conduction in h-BN is achieved by phonon transport, the thermal conductivity of h-BN matrix composite ceramics can be evaluated by Eq. (5) [35. 36]:

$$k = \frac{1}{3} C_p v l \tag{5}$$

where k is the thermal conductivity by phonon transport, C_p is the specific heat capacity of the materials which increase with increasing the temperature, v is the

velocity of phonons which is influenced by the grain orientation and *l* is the mean free path of phonons which is influenced by both the temperature and grain size.

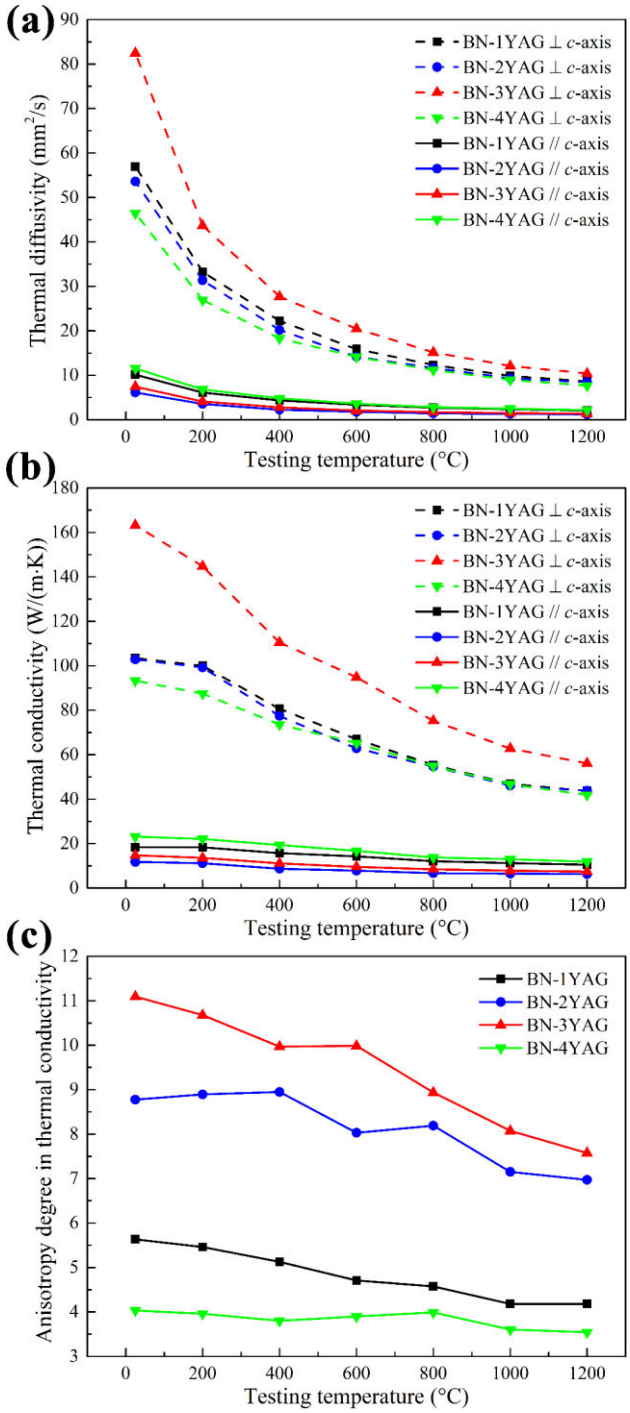

Fig. 9. (a) Thermal diffusivity and (b) thermal conductivity parallel and perpendicular to the *c*-axis orientation and (c) the anisotropy degrees in thermal conductivity of the hot-pressed h-BN matrix composite ceramics with different YAG contents.

With increasing the testing temperature from the room temperature, the number

of phonons increases dramatically, which causes more scattering between phonons and phonons, leading to the decrease of *l*. Further increase of the temperature diminishes *l* to be closer to the lattice spacing, thus the adverse effect of temperature on the thermal conductivity decreases. For the thermal conduction parallel to the *c*-axis orientation, the grain size (the thickness of plate-like h-BN grains) is very small, thus there exist many phonon scattering phenomena caused by grain boundaries, that is, many phonons get scattered by grain boundaries before encountering other phonons. Therefore, the decrease rate of the thermal diffusivity and thermal conductivity parallel to the *c*-axis orientation is slower than that perpendicular to the *c*-axis orientation, which also leads to the decrease of the anisotropy degree in the thermal diffusivity and thermal conductivity with increasing the temperature, especially for BN-3YAG having the highest texture degree (Fig. 9(c)).

Conclusion

Textured h-BN matrix composite ceramics with *in situ* formed YAG were fabricated by hot-pressing using $3Y_2O_3$-$5Al_2O_3$ (mole ratio of 3:5) as the liquid phase sintering additive. The YAG phase was observed to have good wettability to h-BN grains, and a coherent relationship between h-BN and YAG was observed with $[010]_{h\text{-}BN}$ // $[\bar{1}11]_{YAG}$ and $(002)_{h\text{-}BN}$ // $(321)_{YAG}$. The influence of YAG contents on the texture and anisotropy of the composite ceramics were investigated. The rotation of plate-like h-BN grains under the action of the uniaxial pressure in the liquid YAG phase during hot-pressing led to textured microstructures with the *c*-axis of h-BN grains oriented parallel to the sintering pressure, which give these composite ceramics

anisotropy in the mechanical and thermal properties. These textured h-BN matrix composite ceramics behaved a non-catastrophic fracture mode when the crack propagates through h-BN layers, among which the specimen with 30 wt.% YAG content has the highest work of fracture (155.7 ± 5.1 J/m^2) due to its highest texture degree. Further increase of the YAG content (40 wt.%) resulted in the aggregation of liquid YAG phase which caused the buckling of h-BN plates and significantly reduced the texture degree. The specimen with 30 wt.% YAG content also has the most anisotropic thermal diffusivity and thermal conductivity (7.4 mm^2/s and 82.4 mm^2/s, 14.7 W/(m·K) and 163.2 W/(m·K) parallel and perpendicular to the *c*-axis orientation at 25 °C, respectively), making it a promising candidate as thermal management devices in electronics.

Acknowledgement

This work was supported by the National Natural Science Foundation of China (Nos. 52072089, 51832002, 51602074, 51672060) and Heilongjiang Touyan Team Program.

References

[1] L. Song, L. Ci, H. Lu, P.B. Sorokin, C. Jin, J. Ni, A.G. Kvashnin, D.G. Kvashnin, J. Lou, B.I. Yakobson, P.M. Ajayan, Large scale growth and characterization of atomic hexagonal boron nitride layers, Nano Lett. 10(8) (2010) 3209-15.

[2] Y.T. Zheng, H.B. Li, T. Zhou, Microstructure and mechanical properties of h-BN-SiC ceramic composites prepared by in situ combustion synthesis, Mater.

Sci. Eng. A 540 (2012) 102-106.

[3] W.-W. Wu, M. Estili, T. Nishimura, G.-J. Zhang, Y. Sakka, Machinable ZrB_2-SiC-BN composites fabricated by reactive spark plasma sintering, Mater. Sci. Eng. A 582 (2013) 41-46.

[4] L. Xiao, W.J. He, Y.S. Yin, First-Principles Calculations of Structural and Elastic Properties of Hexagonal Boron Nitride, Adv. Mater. Res. 79-82 (2009) 1337-1340.

[5] Z. Zhang, X. Duan, B. Qiu, Z. Yang, D. Cai, P. He, D. Jia, Y. Zhou, Preparation and anisotropic properties of textured structural ceramics: A review, J. Adv. Ceram. 8(3) (2019) 289-332.

[6] X.M. Duan, M.R. Wang, D.C. Jia, N. Jing, Z.L. Wu, Z.H. Yang, Z. Tian, S.J. Wang, P.G. He, Y.J. Wang, Y. Zhou, Anisotropic mechanical properties and fracture mechanisms of textured h-BN composite ceramics, Mater. Sci. Eng. A 607 (2014) 38-43.

[7] P. Jiang, X. Qian, R. Yang, L. Lindsay, Anisotropic thermal transport in bulk hexagonal boron nitride, Phys. Rev. Mater. 2(6) (2018).

[8] W. Yan, Y. Zhang, H. Sun, S. Liu, Z. Chi, X. Chen, J. Xu, Polyimide nanocomposites with boron nitride-coated multi-walled carbon nanotubes for enhanced thermal conductivity and electrical insulation, J. Mater. Chem. A 2(48) (2014) 20958-20965.

[9] J. Eichler, C. Lesniak, Boron nitride (BN) and BN composites for high-temperature applications, J. Eur. Ceram. Soc. 28(5) (2008) 1105-1109.

[10] H. Fang, S.-L. Bai, C.P. Wong, “White graphene” – hexagonal boron nitride based polymeric composites and their application in thermal management, Compos. Commun. 2 (2016) 19-24.

[11] M.J. Meziani, W.-L. Song, P. Wang, F. Lu, Z. Hou, A. Anderson, H. Maimaiti, Y.-P. Sun, Boron Nitride Nanomaterials for Thermal Management Applications, Chemphyschem 16(7) (2015) 1339-1346.

[12] X. Li, Y. Long, L. Ma, J. Li, J. Yin, W. Guo, Coating performance of hexagonal boron nitride and graphene layers, 2D Mater. 8(3) (2021) 034002.

[13] Z. Zhang, S. Hu, J. Chen, B. Li, Hexagonal boron nitride: a promising substrate for graphene with high heat dissipation, Nanotechnology 28(22) (2017) 225704.

[14] Z. Zhu, P. Wang, P. Lv, T. Xu, J. Zheng, C. Ma, K. Yu, W. Feng, W. Wei, L. Chen, Densely packed polymer/boron nitride composite for superior anisotropic thermal conductivity, Polym. Compos. 39(S3) (2018) E1653-E1658.

[15] A. Wilk, P. Rutkowski, D. Zientara, M.M. Bucko, Aluminium oxynitride-hexagonal boron nitride composites with anisotropic properties, J. Eur. Ceram. Soc. 36(8) (2016) 2087-2092.

[16] Z. Shi, J. Wang, G. Qiao, Z. Jin, Effects of weak boundary phases (WBP) on the microstructure and mechanical properties of pressureless sintered Al_2O_3/h-BN machinable composites, Mater. Sci. Eng. A 492(1) (2008) 29-34.

[17] J. Chen, J. Chen, Formation and thermal stability of dual glass phases in the h-BN/SiO_2/Yb-Si-Al-O composites, J. Eur. Ceram. Soc. 40(2) (2020) 456-462.

[18] J.J. Chen, J.X. Chen, X. Zhang, M.M. Hu, M.S. Li, Fabrication and mechanical

properties of h-BN based composites containing dual glass phases, J. Eur. Ceram. Soc. 38(9) (2018) 3210-3216.

[19] Z. Zhang, X. Duan, B. Qiu, Z. Yang, D. Cai, P. He, D. Jia, Y. Zhou, Anisotropic properties of textured h-BN matrix ceramics prepared using $3Y_2O_3$-$5Al_2O_3$(-4MgO) as sintering additives, J. Eur. Ceram. Soc. 39(5) (2019) 1788-1795.

[20] X. Zhang, J. Chen, X. Li, J. Zhang, D. Wan, Y. Zhou, Microstructure and mechanical properties of h-BN/Y_2SiO_5 composites, Ceram. Int. 41(1) (2015) 1279-1283.

[21] T. Kusunose, T. Sekino, Thermal conductivity of hot-pressed hexagonal boron nitride, Scripta Mater. 124 (2016) 138-141.

[22] J. Chen, J. Chen, H. Zhang, M. Hu, M. Li, Microstructure and mechanical properties of h-BN/$Yb_4Si_2O_7N_2$ composites, J. Adv. Ceram. 7(4) (2018) 317-324.

[23] B. Qiu, X. Duan, Z. Zhang, C. Zhao, B. Niu, P. He, D. Cai, L. Chen, Z. Yang, Y. Wang, D. Jia, Y. Zhou, Microstructural evolution of h-BN matrix composite ceramics with La-Al-Si-O glass phase during hot-pressed sintering, J. Adv. Ceram. (2021).

[24] D.W. Ni, G.J. Zhang, Y.M. Kan, Y. Sakka, Textured h-BN Ceramics Prepared by Slip Casting, J. Am. Ceram. Soc. 94(5) (2011) 1397-1404.

[25] J.X. Xue, J.X. Liu, B.H. Xie, G.J. Zhang, Pressure-induced preferential grain growth, texture development and anisotropic properties of hot pressed hexagonal boron nitride ceramics, Scripta Mater. 65(11) (2011) 966-969.

[26] Z. Zhang, X. Duan, B. Qiu, L. Chen, P. Zhang, D. Cai, P. He, H. Zhang, Z. Wei, Z. Yang, D. Jia, Y. Zhou, Microstructure evolution and grain growth mechanisms of h-BN ceramics during hot-pressing, J. Eur. Ceram. Soc. 40(6) (2020) 2268-2278.

[27] X. Duan, D. Jia, Z. Wang, D. Cai, Z. Tian, Z. Yang, P. He, S. Wang, Y. Zhou, Influence of hot-press sintering parameters on microstructures and mechanical properties of h-BN ceramics, J. Alloys Compd. 684 (2016) 474-480.

[28] Z. Zhang, X. Duan, B. Qiu, L. Chen, D. Cai, P. He, Z. Yang, D. Jia, Y. Zhou, Improvement of grain size and crystallization degree of LPSed h-BN composite ceramics by amorphization/nanocrystallization of raw h-BN powders, J. Alloys Compd. 852 (2021) 156765.

[29] M. Hubäĉek, M. Ueki, T. Sató, Orientation and Growth of Grains in Copper-Activated Hot-Pressed Hexagonal Boron Nitride, J. Am. Ceram. Soc. 79(1) (1996) 283-285.

[30] F.K. Lotgering, Topotactical reactions with ferrimagnetic oxides having hexagonal crystal structures—I, J. Inorg. Nucl. Chem. 9(2) (1959) 113-123.

[31] R. Pavlacka, R. Bermejo, Y.F. Chang, D.J. Green, G.L. Messing, Fracture Behavior of Layered Alumina Microstructural Composites with Highly Textured Layers, J. Am. Ceram. Soc. 96(5) (2013) 1577-1585.

[32] H. Yagi, T. Yanagitani, T. Numazawa, K. Ueda, The physical properties of transparent $Y_3Al_5O_{12}$, Ceram. Int. 33(5) (2007) 711-714.

[33] P.H. Klein, W.J. Croft, Thermal Conductivity, Diffusivity, and Expansion of

Y_2O_3, $Y_3Al_5O_{12}$, and LaF_3 in the Range 77°–300°K, J. Appl. Phys. 38(4) (1967) 1603-1607.

[34] W. Paszkowicz, J.B. Pelka, M. Knapp, T. Szyszko, S. Podsiadlo, Lattice parameters and anisotropic thermal expansion of hexagonal boron nitride in the 10-297.5 K temperature range, Appl. Phys. A: Mater. Sci. Process.75(3) (2002) 431-435.

[35] G.A. Slack, R.A. Tanzilli, R.O. Pohl, J.W. Vandersande, The intrinsic thermal conductivity of AIN, J. Phys. Chem. Solids 48(7) (1987) 641-647.

[36] K. Watari, K. Ishizaki, T. Fujikawa, Thermal conduction mechanism of aluminium nitride ceramics, J. Mater. Sci. 27(10) (1992) 2627-2630.